Fall 2011

Temperature elevations due to NIR exposure in the brain tissue

Ali Ersen
New Jersey Institute of Technology

Copyright Warning & Restrictions

The copyright law of the United States (Title 17, United States Code) governs the making of photocopies or other reproductions of copyrighted material.

Under certain conditions specified in the law, libraries and archives are authorized to furnish a photocopy or other reproduction. One of these specified conditions is that the photocopy or reproduction is not to be "used for any purpose other than private study, scholarship, or research." If a, user makes a request for, or later uses, a photocopy or reproduction for purposes in excess of "fair use" that user may be liable for copyright infringement,

This institution reserves the right to refuse to accept a copying order if, in its judgment, fulfillment of the order would involve violation of copyright law.

Please Note: The author retains the copyright while the New Jersey Institute of Technology reserves the right to distribute this thesis or dissertation

Printing note: If you do not wish to print this page, then select "Pages from: first page # to: last page #" on the print dialog screen

ABSTRACT

TEMPERATURE ELEVATIONS DUE TO NIR EXPOSURE IN THE BRAIN TISSUE

by
Ali Ersen

Near infrared (NIR) lasers have been used in medical applications both for diagnostic and therapeutic purposes. Temperature elevation profile inside the tissue is a critical factor that needs to be better understood in these applications. The purpose of this study is to determine the temperature distribution due to a low power NIR laser irradiation in living neural tissue. Temperature measurements were made directly using a thermocouple probe inside the rat brain cortex within the sagittal plane. The spatial map indicates that NIR light penetrates more readily in the vertical directions than the spreading in the horizontal axis. The decrease in the vertical direction can be approximated with a single order exponentially decaying function. The results also suggest that the temperature elevation can be kept below 0.5 °C anywhere in the tissue if the incident laser beam power density is less than 27 mW/cm^2. These experiments should be repeated in other types of neural tissue such as the white matter of the brain and the spinal cord to obtain more complete results.

TEMPERATURE ELEVATIONS DUE TO NIR EXPOSURE IN THE BRAIN TISSUE

by
Ali Ersen

A Thesis
Submitted to the Faculty of
New Jersey Institute of Technology
in Partial Fulfillment of the Requirements for the Degree of
Master of Science in Biomedical Engineering

Department of Biomedical Engineering

January 2012

APPROVAL PAGE

TEMPERATURE ELEVATIONS DUE TO NIR EXPOSURE IN THE BRAIN TISSUE

Ali Ersen

Dr. Mesut Sahin, Dissertation Advisor — Date
Associate Professor of Biomedical Engineering, NJIT

Dr. Bryan J. Pfister, Committee Member — Date
Associate Professor of Biomedical Engineering, NJIT

Dr. Yahia M. Al-Smadi, Committee Member — Date
Senior Mechanical Engineer, Special Practices Group
AECOM, New York, NY 10005

BIOGRAPHICAL SKETCH

Author: Ali Ersen

Degree: Master of Science

Date: January 2012

Undergraduate and Graduate Education:

- Master of Science in Biomedical Engineering,
  New Jersey Institute of Technology, Newark, NJ, 2012

- Bachelor of Science in Electronics Engineering,
  Erciyes University, Kayseri, Turkey, 2006

Major: Biomedical Engineering

Presentations and Publications:

Ammar Abdo, Ali Ersen, Mesut Sahin, "Temperature Elevation inside Neural Tissue Illuminated by NIR Laser", 33rd Annual International IEEE EMBS Conference (EMBS'11), Boston, MA, USA, August 2011.

‘My Lord, increase me in knowledge.’ (20:114)

ACKNOWLEDGMENT

I would like to thank Dr. Mesut Sahin for his supervision, guidance and advice. Without his support, this study would have been much harder and taken longer time. I would also like to acknowledge Dr. Bryan J. Pfister and Dr. Yahia Al-Smadi for actively participating in the committee. I am grateful to Ammar Abdo for his assistance in experiments and special thanks to Gokhan Ordek for his help.

I would like to thank my family for their encouragement.

Financial support for this work was provided by a grant from National Institute of Health.

TABLE OF CONTENTS

Chapter	Page
1 INTRODUCTION ……...……..…….……..….	1
1.1 Temperature Measurement …….…….……...…...	1
1.1.1 Contact Methods …….…….……	1
1.1.1.1 Thermocouples…….…….	1
1.1.1.2 Resistive Thermal Devices (RTDs) ……..……...	3
1.1.1.3 Thermistors……...	4
1.1.1.4 Fiber Optic Probes……	5
1.1.1.5 Integrated Circuit Temperature Transducers ……...…	6
1.1.2 Non-Contact Methods ..……	10
1.1.2.1 Infrared (IR) Thermometers……..	10
1.1.2.2 Laser Scattering Methods…….…….	12
1.1.2.3 Pyrometers…….....	13
1.2 Infrared (IR) Imaging…..…….…..…….……	13
1.2.1 Infrared Imaging in Medicine …...…….……...	13
1.3 The Laser Intensity Profile .……...	15
1.3.1 Transverse Electromagnetic (TEM) Modes…….……..	15

TABLE OF CONTENTS
(Continued)

Chapter **Page**

1.3.2 Gaussian Intensity Profile……. 16

1.4 Heat Transfer Mechanism in Biological Tissue ……. 19

1.4.1 Bioheat Equations…….…..…….…….. 19

1.4.2 Optical Properties of Tissue…….. 21

2 METHODOLOGY ……..…….…….……. 22

2.1 Temperature Probe Calibration ...…….……...… 22

2.2 Laser Calibration …...……..…... 23

2.3 Animal Anesthesia …….…… 24

2.4 Computer Interface ……..…...…… 24

2.4.1 Pre Amplification …….…… 25

2.4.2 DAQ Board …….…….……..... 26

2.4.3 Custom Software …….…….……..... 26

2.5 Experimental Procedure….…….…… 27

3 RESULTS and DISCUSSION ……..…….…… 31

3.1 Thermocouple Calibration…….……...…….…….. 31

3.2 Laser Calibration …….……....…….…… 32

TABLE OF CONTENTS
(Continued)

Chapter **Page**

3.3 Experimental Results and Discussion ……....……. 33

3.4 Limitations……...……....……. 41

4 SUMMARY and FUTURE WORK ……..…… 43

APPENDIX MATLAB SOURCE CODES FOR THE TEMPERATURE DIFFERENCE DETERMINATION …….. 46

REFERENCES ……..……..… 53

LIST OF TABLES

Table		Page
1.1	Comparisons of Different Types of Temperature Sensors ……	6
1.2	Thermo-physical Properties of Human Tissue and Water …….	21
2.1	Specifications for T301……...	22

LIST OF FIGURES

Figure		Page
1.1	Basic thermocouple circuit	2
1.2	Platinum film RTD	3
1.3	A typical circuit for temperature measurement with a thermistor	4
1.4	Fiber optic thermometry probe	5
1.5	AD590 temperature sensor	8
1.6	Infrared gun thermometers	11
1.7	An example of commercial pyrometer	12
1.8	Thermal image of woman's abdomen taken by a Duracam infrared camera	13
1.9	Transverse electromagnetic modes	15
1.10	Gaussian intensity profile of a laser beam determination of the spot size	18
2.1	T301 digital thermometer unit	22
2.2	Block diagram of the laser control and temperature acquisition into the computer via the NI DAQ board	25
2.3	A non-inverting amplifier with a gain of 41	25
2.4	NI PCI 6259 DAQ board, maximum sampling frequency is 1.25 MHz	26
2.5	The custom Matlab software user interface	27
2.6	Exposed area of the cerebral cortex for temperature measurements in the experimental animals	28
2.7	The modified thermocouple probe	28
2.8	Experiment setup including laser thermocouple and the stereotaxic frame	29
2.9	The laser control pattern and recorded temperature change	30

LIST OF FIGURES
(Continued)

Figure		Page
3.1	Temperature calibration curve …..……..……..…….	31
3.2	Control voltage vs. output power of the laser measured experimentally ……...	32
3.3	An example of raw temperature data collected at a depth of 500 μm…..……..	33
3.4	The temperature measurements at the beginning and end of the laser pulse …….	34
3.5	The map of the temperature elevation in experiment 5 ……...……...…….	35
3.6	The map of the temperature elevation in experiment 6 ……..…..…….....	36
3.7	The map of the temperature elevation in experiment 7 ……...……...…….	37
3.8	The map of the temperature elevation in experiment 8 ……...……...…….	38
3.9	The average temperature increase profile of neural tissue in the vertical plane (sagittal) due to laser illumination ..…..……	39
3.10	The temperature elevation as a function of depth in the rat brain due to NIR laser exposure ……...……..……...	41

CHAPTER 1

INTRODUCTION

1.1 Temperature Measurement

Accurate temperature measurement plays an important role in many biological applications and these applications require temperature sensors with different characteristics. There are some specifications that need to be satisfied by the sensor technology; for instance the size of the sensor, temperature measuring range, long term stability, accuracy, response time, affordability, and reproducibility of the measurements [1]. The methods of temperature measurement are in general classified under two categories: Contact and Non-Contact methods.

1.1.1 Contact Methods

Contact methods require some parts of the temperature sensor to be in contact with the object, the temperature of which to be measured, and sample the temperature through conduction. These systems require the sensor probe to be robust in order to protect its integrity in corrosive environments.

1.1.1.1 Thermocouples. When two metals are connected together, a thermoelectric voltage is produced due to different binding energies of the electrons to the metal ions. This voltage depends on the type of the metals as well as the temperature. In order for this thermal voltage to produce a flow of current, the two metals must also be joined together at the other end so that a closed circuit is formed. The thermoelectric effect was

discovered in 1822 by Seebeck, and as early as 1828 Becquerel recommended the use of platinum- palladium thermocouples for temperature sensing.

If the temperatures at the two end junctions are the same, there is not a voltage difference since the individual voltages produced at these two points cancel each other. With different temperatures at the junctions, the voltages generated are different and a current flows. Thermocouples can thus only measure temperature differences. The measurement point is the junction that is exposed to the temperature to be measured. The reference junction is the junction at the known temperature. Since the known temperature is usually lower than the measured temperature, the reference junction is generally called the `cold junction`. In order to calculate the actual temperature at the measurement point, the cold junction temperature must be known. Older instruments used a thermostatically controlled junction box to control this cold junction temperature at a known value, e.g. 50 °C. Modern instruments use a thin film Resistive Thermal Device (RTD) at the cold junction to determine its temperature or an electronic cold junction circuit and calculate the measurement point temperature. The voltage produced by the thermoelectric effect is very small and amounts to only a few microvolts per degree Celsius. Thermocouples are therefore not generally used below the freezing point since the difference from the reference junction temperature is too small to produce an interference-free signal [2].

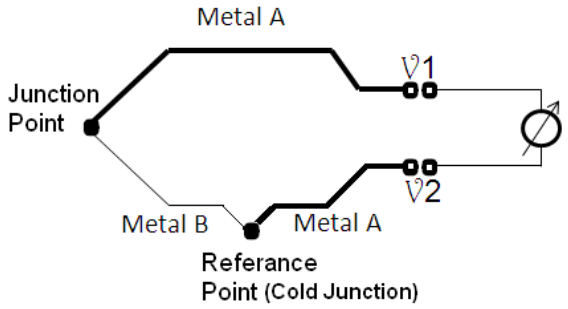

Figure 1.1 Basic thermocouple circuit [2]

1.1.1.2 Resistive Thermal Devices (RTDs). The electrical conductivity of a metal depends on the mobility of the charge carriers. If a voltage is applied to the ends of a metal wire, the electrons move to the positive pole. Faults in the crystal lattice interfere with this movement. They include foreign or missing lattice atoms, grain boundaries, and atoms on interlattice positions. Since these fault positions are independent of temperature they produce a constant resistance. With rising temperature, the atoms of the metal lattice exhibit increasing oscillations about their rest positions and thereby impede the movement of the conduction electrons. Since this oscillation increases linearly with temperature, the resistance increase caused by it depends as a first approximation directly on the temperature.

In RTDs, the electrical resistance of the metal increases with temperature, i.e. it is a Positive Temperature Coefficient (PTC) sensor. The most common metals in use are platinum and nickel. The most commonly used sensor is the 100 or 1000 Ohm platinum RTD. RTDs are the most accurate sensors for industrial applications and also preferred for their superior long-term stability. After one year, there may be a shift of +0.05 °C through aging. Platinum RTDs can cover a temperature range from -200 to 800 °C [3].

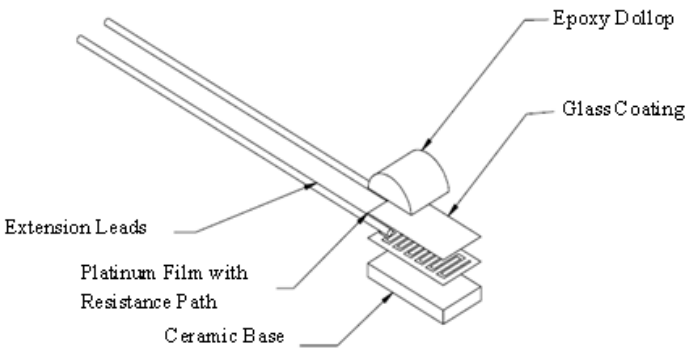

Figure 1.2 Platinum film RTD [4]

1.1.1.3 Thermistors. Thermistors are made from certain metal oxides whose resistance decrease with increasing temperature. Because the resistance value falls off with increasing temperature they are called negative temperature coefficient (NTC) sensors. Due to the nature of the basic process the number of conducting electrons increases exponentially with temperature; the characteristic therefore exhibits a sharp rising curve. This pronounced non-linearity is a disadvantage of NTC resistors and limits their useful temperature span to about 100 °C. They can be linearized with a look up table stored in a computer memory. However, accuracy and linearity generally do not meet the requirements over large measurement ranges. Their drift under varying temperatures is also larger than that of RTDs. Their field of use is limited to monitoring and indicator applications where the temperature does not exceed 200 °C. In less demanding applications, they are usually preferable to more expensive thermocouples and RTDs due to their low cost and relatively simpler electronic circuitry that they require. In addition, thermistors can be manufactured in very small designs with a small mass which in turn results in a fast response time [5]. As shown in Figure 1.3, thermistors can be interfaced with an analog-to-digital converter directly without an amplification stage since the resistance change per degree Celsius is quite large.

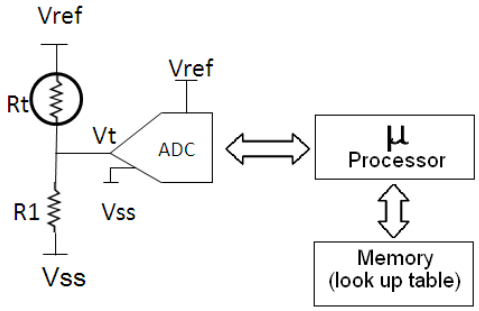

Figure 1.3 A typical circuit for temperature measurements with a thermistor

1.1.1.4 Fiber Optic Probes. Fiber-optic sensors are contact type sensors where laser light is passed through a light guide that is placed in the medium where the temperature is to be measured. The thermal expansion of the light guide changes the parameters of the index of refraction allowing interferometry of laser signals to provide a measure of temperature. While this method yields measurements with excellent resolution, the temperature ranges and time constants are limited due to material specifications. This method has been used successfully up to temperature values of 1600 °K [6]. Because the light guide usually need to be of a certain length in order to achieve sufficient sensitivity, these types of sensors are not appropriate for point measurements.

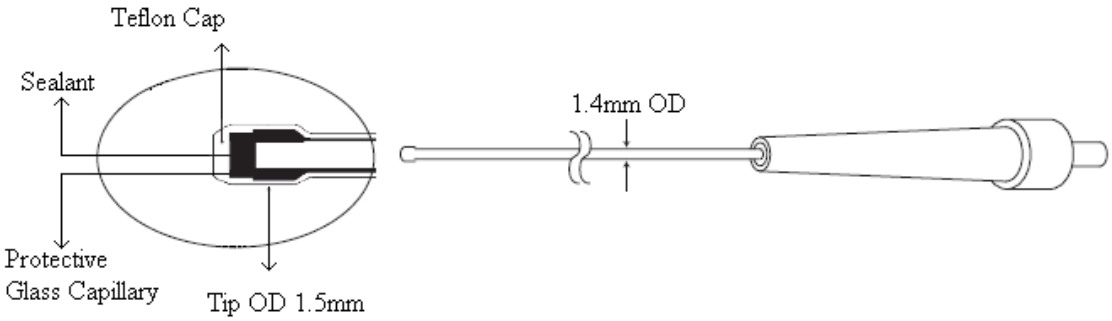

Figure 1.4 Fiber optic thermometry probe [6]

1.1.1.5 Integrated Circuit Temperature Transducers. Semiconductor temperature sensors are produced in the form of Integrated Circuits (IC). Their design is based on the fact that semiconductor diodes have temperature-sensitive voltage vs. current characteristics. When two identical transistors are operated at a constant ratio of collector currents, the difference in base-emitter voltages is directly proportional to the absolute temperature.

Table 1.1 Comparisons of Different Types of Temperature Sensors [7]

	Thermocouples	RTD`s	Thermistors	Fiber Optic Probes
Accuracy	Accurate	More Accurate	Less Accurate	Less Accurate
Temperature Range	-250 °C to +2600 °C	-200 °C to +850 °C	-60 °C to +300 °C	-50 °C to +3000 °C
Stability (Drift)	Reasonable for limited lifetime	Good	Good	Good
Repeatability	Reasonable	Good	Good	Good
Hysteresis	Excellent	Good	Good	Good
Vibration	Very Resistant	Less Resistant	Good	Tolerant
Measurement Area	Single Point	Whole RT Element	Whole bead (Small)	Varies
Diameter	Small Sizes (to 0.25mm)	Larger (3.0mm min)	Small (0.5mm min)	Varies
Linearity	Linear in a large range	Linear	Not Linear	Reasonably Linear
Reference Junction	Required	Not Required	Not Required	Not Required
Lead Wire Resistance	No Problem	Must be Considered	No Problem	Not Required
Contact Required	Yes	Yes	Yes	Yes
Response	Fast	Slower	Medium	Fast, still slower than thermocouples

The use of IC temperature sensors is limited to applications where the temperature varies within a –55 to 150 °C range. The measurement range of IC temperature sensors may be small compared to that of thermocouples and RTDs, but they have several advantages: they are smaller than fiber optic probes, more accurate than thermocouples, inexpensive, and are easy to interface with electronic devices such as amplifiers, Digital Signal Processors (DSP), and microcontrollers.

The earliest type of IC temperature sensor improved on the existing thermistor solutions whose resistance varied with temperature in a nonlinear fashion. Modern analog temperature sensors eliminated the need for additional linearization circuitry to correct for thermistor nonlinearity.

IC temperature sensors continue to evolve, providing an array of functions, features, and interfaces. With the higher level of integration now feasible, digital IC temperature sensors can report both local and remote temperatures, monitor other system parameters, control fans, or warn when a specific temperature is exceeded.

There are two main types of IC temperature sensors: analog and digital in addition several variations of each type. Analog sensors can produce a voltage or current proportional to temperature. Digital sensors may monitor local and/or remote temperatures, and can also include features such as voltage monitoring, fan control, and over- or under-limit alarms.

Digital temperature sensors are similar to analog temperature sensors, but instead of outputting the data in current or voltage, it is converted into a digital format of 1's and 0's. Digital-output temperature sensors are therefore particularly useful when interfacing to a microcontroller [8].

While newer digital output temperature sensors have replaced analog output temperature sensors in many applications, analog temperature sensors continue to find a home in applications that do not require a digitized output. For example, the AD590 sensor is still a viable product in many applications more than 25 years after its release, and it is often used in remote applications as its high-impedance current output makes it insensitive to voltage drops over long lines. It can be used in a wide variety of

temperature-sensing applications not only because it operates up to 150 °C, but also because of its wide operating voltage range (4-30 V).

An example of analog IC temperature transducer is AD590, which is a two-terminal integrated circuit temperature transducer that produces an output current proportional to absolute temperature. For supply voltages between 4 V and 30 V the device acts as high impedance, constant current regulator passing 1 μA/K. Laser trimming of the chip's thin-film resistors is used to calibrate the device to 298.2 μA output at 298.2 K (25 °C).

Figure 1.5 AD590 temperature sensor [9]

The AD590 can be used in any temperature sensing application below 150 °C in which conventional temperature sensors are currently employed. The inherent low cost of a monolithic integrated circuit combined with the elimination of support circuitry makes the AD590 an attractive alternative for many temperature measurement situations. Linearization circuitry, precision voltage amplifiers, resistance measuring circuitry and cold junction compensation are not needed in a circuit involving AD590.

In addition to temperature measurement, applications include temperature compensation or correction of discrete components, biasing proportional to absolute temperature, flow rate measurements, level detection of fluids and anemometry. The

AD590 is available in the chip form, making it suitable for hybrid circuits, and fast temperature measurements in protected environments.

The AD590 is particularly useful in remote sensing applications. The device is insensitive to voltage drops over long lines due to its high impedance current output. Any well insulated twisted pair is sufficient for operation hundreds of feet from the electronics. The output characteristics also make the AD590 easy to multiplex: the current can be switched by a CMOS multiplexer or the supply voltage can be switched by a logic gate output [9].

1.1.2 Non- Contact Methods

An accurate measurement and control of temperature can be of great importance in most material manufacturing and processing applications. With recent technology, such measurements almost always require either physical contact with the target or an extensive calibration procedure. The method significantly alters the temperature or other characteristics of the object, or otherwise the sensor is in a hostile environment. Accordingly, calibration may not be possible if the characteristics change too much.

Since using non-contact methods can determine the temperature of a target object without physical contact, the measurement system does not contaminate, damage, or interfere with the process being monitored and has many advantages over contact measurement devices. Non-contact measurement devices can be mounted remotely from the hot target, enabling it to operate for long periods with minimal maintenance. Another significant advantage is the very fast response time provided by non-contact devices; typically a temperature measurement can be made within a few thousandths of a second [10].

1.1.2.1 Infrared (IR) Thermometers. Infrared thermometers measure temperature from a distance. This distance can be many miles or a fraction of an inch. Infrared thermometers are often used in circumstances when other sorts of thermometers are not practical. If an object is very fragile or dangerous to be near, for example, an infrared thermometer is a good way to get a temperature reading from a safe distance.

Infrared thermometers work based on a phenomenon called black body radiation. Any object with a temperature above absolute zero has its molecules moving around. The higher the temperature, the faster the molecules move. As they move, the molecules emit infrared radiation, a type of electromagnetic radiation below the visible spectrum of light. As they get hotter, they emit more infrared, and the peak emission wavelength shifts towards visible light. That is why heated metal can glow red or even white. Infrared thermometers detect and measure this radiation.

Infrared light works like visible light: it can be focused, reflected or absorbed. Infrared thermometers usually use a lens to focus infrared light from one object onto a detector called a thermopile. The thermopile absorbs the infrared radiation and turns it into heat. The more infrared energy, the hotter the thermopile gets. This heat is turned into electricity. The electricity is sent to a detector, which uses it to determine the temperature of the object that the thermometer is pointed at.

Infrared thermometers are adaptable to most temperature measurement applications. Capable of measuring a broad spectrum of temperature ranges from approximately -4 to 7,200 °F (-20 to 4,000 °C), they are available in designs as simple as hand-held point-and-shoot guns with lasers that can output temperature measurements in real time [11].

Figure 1.6 Infrared gun thermometers [12]

1.1.2.2 Laser Scattering Methods. A commonly used method for measuring temperature using a laser is Coherent Anti-Stokes Raman Spectroscopy (CARS), is a non-contact technique capable of providing spatially and temporally resolved measurements of temperature and major species concentration in hostile environments. It is often the only non-contact thermometry technique, which can be applied in many practical combustion rigs, for example primary zones of liquid kerosene combustion rigs, and large coal fired burners. Using multi-photon scattering, molecules interact with multiple photons where the mixing provides sum and difference frequencies at the resonant energies. The resulting Raman spectrum has the sum or difference frequencies coinciding with one of the molecular levels that are then emitted as a third laser beam. This coherent scattering is stronger than incoherent scattering and is useful where there is another emitting background such as in a furnace [13].

CARS is used for species selective microscopy and combustion diagnostics. The first exploits the selectivity of vibrational spectroscopy whereas the latter is aimed at temperature measurements: the CARS signal is temperature dependent. The strength of

the signal scales (non-linearly) with the difference in ground state population and vibrationally excited state population. Since the population of states follows the temperature dependent Boltzmann Distribution, the CARS signal carries intrinsic temperature dependence as well. This temperature dependence makes CARS popular technique for monitoring the temperature of hot gases and flames. More recently, CARS has been utilized as a method for non-invasive imaging of lipids in biological samples both in vivo and in vitro [14].

1.1.2.3 Pyrometers. A pyrometer is a non-contacting device that intercepts and measures thermal radiation, a process known as pyrometry. This device can be used to determine the temperature of an object's surface. A pyrometer projects the images of a blackbody radiator on a photoelectric detector that translates the spectral radiation flux into a photocurrent. This current is then calibrated using a reference standard such as high-stability tungsten strip lamps at different temperatures.

Pyrometers are suited especially for temperature measurements of moving objects or any surfaces that cannot be reached or cannot be touched. Recent advances in pyrometers have increased their range of operation to 700 °C – 4500 °C [15, 16].

Figure 1.7 An example of commercial pyrometer [15]

1.2 Infrared (IR) Imaging

1.2.1 Infrared Imaging in Medicine

Infrared imaging forms an image using infrared radiation and operates in wavelengths as long as 14 μm. This kind of image formation has been a very successful diagnostic tool in the field of medicine. The discovery of infrared imaging has led to reduction of more invasive procedures for diagnosis. The principle on which infrared imaging works is very simple: as the temperature increases, the amount of radiation emitted by an object increases. This imaging method helps us see the variations in temperature. Warm areas appear bright against cooler backgrounds. Generally, any disease in human body is accompanied by inflammation, which is actually a protective mechanism for the body. During inflammation, vascularization increases in the affected area and this in turn leads to an increase in temperature. The increased temperature is utilized by infrared imaging for identifying the disturbance in the normal physiological process.

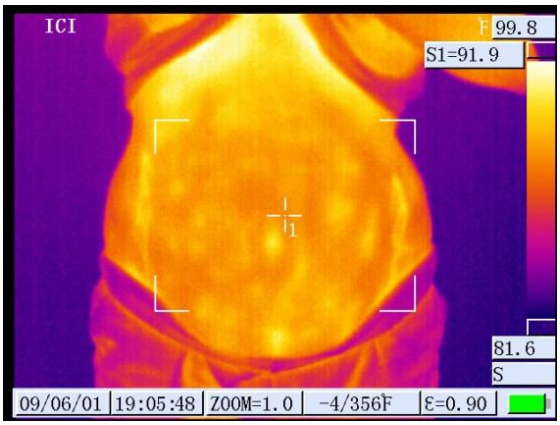

Figure 1.8 Thermal image of woman's abdomen taken with a DuraCam infrared camera [17]

The digital infrared camera produces high-resolution thermal images that are very essential for diagnosis. The medical fields in which Infrared Imaging is used are:

- Oncology- Deals with cancerous lesions. The cancerous and pre-cancerous tissue show an increase in vascularity and temperature in the affected area. The digital infrared camera helps in providing high resolution images and thus very early diagnosis of cancers. This diagnostic tool has been very useful in identifying breast cancers much earlier in cases where even the mammogram thechique has failed.
- Vascular disorders- Deals with bleeding disorders. The digital infrared camera captures any deviation from the normal within a blood vessel. Hemorrhages and clots within blood vessels can be identified by these Infrared cameras.
- Respiratory disorders- Deals with breathing disorders. The digital infrared camera helps in finding out the physiological changes within the respiratory organs.
- Skeletal and neuromuscular diseases- Deals with bones, nerves, and muscle diseases. Even the smallest of hairline cracks within a bone can be captured by digital infrared camera because of its very high resolution. Similarly infrared cameras play a major role in identifying neuromuscular diseases.
- Surgery- Deals with invasive procedures done in order to treat a patient. Infrared cameras give a helping hand to the surgeons to localize the blood vessels when they are performing micro surgeries.
- Tissue viability- Deals with the vitality of tissues. Infrared cameras help in detecting the vitality by ensuring adequate blood supply to the tissues [17].

1.3 The Laser Intensity Profile

1.3.1 Transverse Electromagnetic (TEM) Modes

The radiation emitted by lasers contains several discrete optical frequencies separated from each other by frequency differences which can be associated with different modes of the lasers. The mode is describing the variations in the electromagnetic field along the optical axis of the laser cavity. The electromagnetic field variations perpendicular to the direction of travel of the wave are called "transverse electromagnetic (TEM) modes".

TEM modes in general are specified as TEM_{mn}, where m is the number of dark bands (white areas in Figure 1.9) crossing the horizontal axis and n is the number of dark bands (white areas in Figure 1.9) crossing the vertical axis. Laser will produce an output for all TEM modes for which gain exceeds loss within the laser cavity [19].

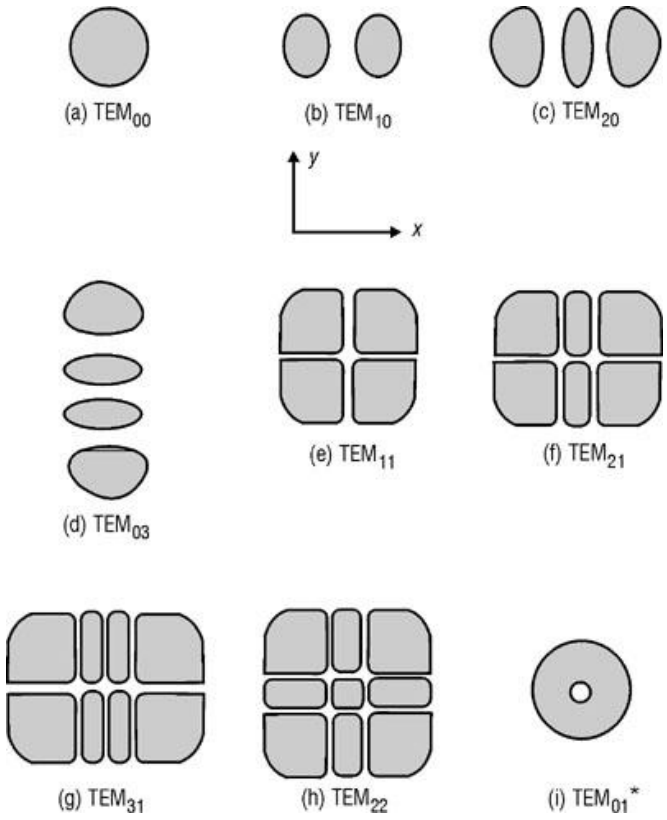

Figure 1.9 Transverse electromagnetic modes [19]

1.3.2 Gaussian Intensity Profile

Most of the lasers that work in TEM_{00} mode would emit a beam with a Gaussian intensity profile. The shape of beam is characteristics of these lasers; it has a lower beam divergence than other modes. Lower divergence is important in the transmission of beams over large distances. For example, it can be focused to a spot smaller than other existing modes. This is important in an application such as drilling. Its spatial coherence is ideal for applications that depend upon the interference of light. Other modes cannot be used because they lack adequate spatial coherence.

Other important specifications include the spot size, a characteristic radius of the Gaussian beam at a particular location along the direction of the propagation of the beam. The decrease of the field amplitude, E(r) with distance r from the axis in a Gaussian beam is written as,

$$E(r) = E_0 e^{\frac{-r^2}{w^2}} \tag{1.1}$$

Equation 1.1 is expressed in polar coordinates where r is the radial distance from the center of the beam and w is a parameter which is called the spot size of the Gaussian beam (it is also referred to as the Gaussian beam radius). The transverse direction is the x-y plane; which is perpendicular to direction of the propagation.

The relation between Intensity I and Electric field E is described by

$$I = \frac{\varepsilon_0 c\, E^2}{2} \tag{1.2}$$

Here $\varepsilon_0 = 8.85*10^{-12}\ \frac{C^2}{N\,m^2}$ is the permittivity of free space and c = $3*10^8$ m/s the speed of the light, so the intensity is calculated by

$$I(r) = I_0\, e^{\frac{-2r^2}{w^2}} \tag{1.3}$$

Figure 1.10 shows the Gaussian intensity profile according to Equation 1.3.

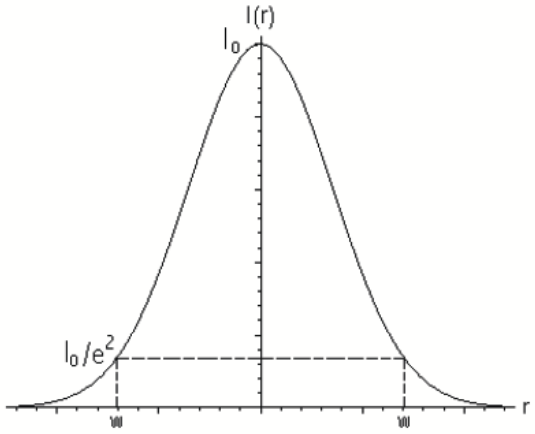

Figure 1.10 Gaussian intensity profile of a laser beam and definition of the spot size

When r is equal to w, the intensity is $\frac{I_0}{e^2}$. This shows that at a distance w from the z axis, the intensity of light is reduced to $\frac{1}{e^2}$ of its maximum value. If a screen is placed perpendicular to the z-axis at this position, a spot of radius ~w would be observed. The spot size is a function of position along the direction of propagation (z). It is given by

$$w(z) = w_o \cdot \sqrt{1 + \left(\frac{\lambda z}{\pi w_0^2}\right)^2} \quad (1.4)$$

Here, λ is the wavelength of the light. It should be mentioned that w_0 is the minimum spot size which occurs at z=0. The size of the beam at z=0 is called the beam waist.

Although the spot size and the radius of curvature vary along the z-axis, the intensity profile remains Gaussian at every position along the direction of propagation. In fact, Gaussian beams have a unique property that maintains their Gaussian form along their propagation direction. At distances far away from the source, the beam profile changes because of the diffraction [20, 25].

1.4 Heat Transfer Mechanisms in Biological Tissue

The heat transfer in living tissue is a complex process involving multiple mechanisms including blood perfusion, conduction, metabolism, and propagation. These complexities make determining the thermal properties a technically challenging task. And also, it is difficult but necessary to decouple these different heat transfer mechanisms.

The blood-tissue heat interaction is a set of parameters including perfusion rate, vascular anatomy and different tissues of the body with or without pathology.

Once a system has a significant difference between temperature of blood and tissue through which it flows, conductive heat transport will occur.

The analysis of the effect of blood perfusion on the temperature distribution in living tissue remains a topic of active research [21].

1.4.1 Bioheat Equation

Principles of engineering and laws of physics and chemistry in general terms including biological tissue properties describe Bioheat transfer. In calculations of heat transportation and temperature rise in perfused media, a linear bioheat transfer equation initially proposed by Pennes is used [22,23]. In an assessment by Eberhart [24] it is concluded that this equation is an adequate model for prediction of the macroscopic temperature distribution in several biological tissues.

The bioheat equation is similar to the generic heat equation for heat conduction except that it splits the heat-source term on the right-hand side into three terms that are of interest in bioheat transfer problems. Further, the material properties in this equation need to be chosen carefully for the tissue type studied. The equation thus takes the form:

$$\delta_{ts}\rho C\frac{\partial T}{\partial t} + \nabla . \left(-k\nabla T\right) = \rho_b C_b \omega_b \left(T_b - T\right) + Q_{met} + Q_{ext} \tag{1.6}$$

where

δ_{ts} is a time- scaling coefficient (dimensionless)

ρ is the tissue density (kg/m^3)

C is the specific heat of tissue (J/(kg.K))

k is the tissue's thermal conductivity tensor (W/(m.K))

On the right side of the equation, $\rho_b C_b \omega_b \left(T_b - T\right)$ is a source term for the blood perfusion where:

ρ_b is the density of the blood (kg/m^3)

C_b is the specific heat of the blood (J/(kg.K))

ω_b is the blood perfusion rate ($m^3/(m^3.s)$)

T_b is the arterial blood temperature (K)

The second and third terms on the right side are:

Q_{met}, the heat source from metabolism (W/m^3)

Q_{ext}, the spatial heat source (W/m^3)

For the steady-state problem, the temperature does not change over time, and the first term in bioheat equation disappears from the left side. The typical values for some tissue parameters are comparing with water in Table 1.2.

Table 1.2 Thermo-physical Properties of Human Tissue and Water [41]

Material	Conductivity $(W\ m^{-1}K^{-1})$	Density $kg\ m^{-3}\ .10^{-3}$	Specific heat $(kJ\ kg^{-1}K^{-1})$
Muscle	0.38-0.54	1.01-1.05	3.6-3.8
Fat	0.19-0.20	0.85-0.9	2.2-2.4
Kidney	0.54	1.05	3.9
Heart	0.59	1.06	3.7
Liver	0.54	1.05	3.6
Brain	0.16-0.57	1.04-1.05	3.6-3.7
Water at 37°C	0.63	0.99	4.2

1.4.2 Optical Properties of Tissue

When light interacts with tissue, it is both absorbed and scattered in various proportions depending on the optical properties of the tissue. The tissue characteristics are important for all kinds of medical laser applications, in order to understand the interaction mechanisms between light and tissue. In this study, light is considered as NIR laser beam and the tissue is neural tissue of the brain cortex, which mostly the gray matter.

The values for the gray matter are 0.47 cm^{-1} [28] for the absorption coefficient, 51 cm^{-1} [28] for the scattering coefficient, g=0.9 [29] for the anisotropy factor, and 1.38 [29] for the refractive index. The absorption coefficient for the white matter is 0.64 cm^{-1} [28] and the scattering coefficient is 265 cm^{-1} [28]. We cite these values here as a reference for the reader. No computer modeling is built in this study.

CHAPTER 2

METHODOLOGY

2.1 Temperature Probe Calibration

In this study to get reliable and accurate results, a T type (Cu-CuNi) thermocouple sensor is used. The temperature micro sensor by Unisense, (Denmark) is a miniaturized thermocouple sensor. The thermocouple has a 100 μm tip. The therpotential is amplified and filtered by T301 unit and the output taken as a voltage as well as a reading on a Liquid Crystal Display (LCD).

Table 2.1 Specifications for T301

Voltage Supply	9 V Battery
Range	-80.0 / +199.9 °C
Input	Cu-CuNi
Output	5 mV/°C

The calibration of the sensor is done in water while its temperature is being changed slowly. The temperature is measured both by a glass mercury thermometer and T301, observed on glass thermometer scale and T301's digital panel. The voltage output is measured and recorded with a voltmeter as well.

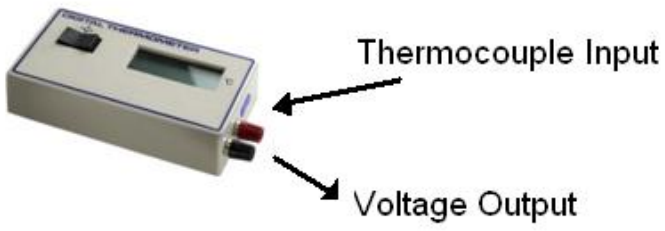

Figure 2.1 T301 Digital thermometer unit

2.2 Laser Calibration

The NIR Laser (DLS-500-830FS-100) source used in this study has a Gaussian profile with a circular footprint and wavelength of 830 nm. The radius was taken at $\sqrt{2}\sigma$ of Gaussian profile, which is the radial distance where the intensity drops down to $1/e^2$ of its peak. The laser spot size was calculated by the Equation 1.4. The spot size is 0.56 mm at z= 13.5 cm from the laser. This diameter corresponds to the diameter of a flat profile beam with the same peak power density and the same total power as the Gaussian profile laser.

The total instantaneous power varied linearly with the control signal, as specified by the laser manufacturer. The power density at the surface of tissue was determined accordingly for a train of pulses using Equation 2.1.

$$\text{Power density} = (P/A) \times PW \times f \qquad (2.1)$$

where

P is the total peak power of the laser source (mW)

A is the cross sectional area of the beam at the targeted tissue (cm^2)

PW is the pulse width (s)

f is the frequency of the control pulse train (Hz)

The (PW x f) product can be substituted by the duty cycle of the pulse train.

2.3 Animal Anesthesia

Eight Sprague-Dawley male rats (350-500 g) were used for this study. Anesthesia was induced with intraperitorial injection of ketamine (80 mg/kg) and xylazine (12 mg/kg) mixture diluted with saline. Ketamine was used in further doses to maintain the anesthesia as needed. Also Marcaine (0.2 mL) was injected at the site of incision as a local anesthetic. Dexamethasone (2 mg/kg) was administered intramuscularly at the beginning of the surgical procedure to prevent edema in the central nervous system. The rectal temperature was continuously monitored and maintained between 35-36 °C using a temperature regulated heating pad. Dehydration of brain tissue was prevented using a pool of warm saline over the exposed area of the brain. All procedures were approved and performed in accordance with the guidelines of the Animal Care and Use Committee, Rutgers University, Newark, NJ.

2.4 Computer Interface

A custom Matlab code [37] was used with National Instruments (NI) DAQ board to send a train of control pulses to the laser and record the temperature values detected by the thermocouple. The computer interface of this setup is shown in Figure 2.2 as a block diagram.

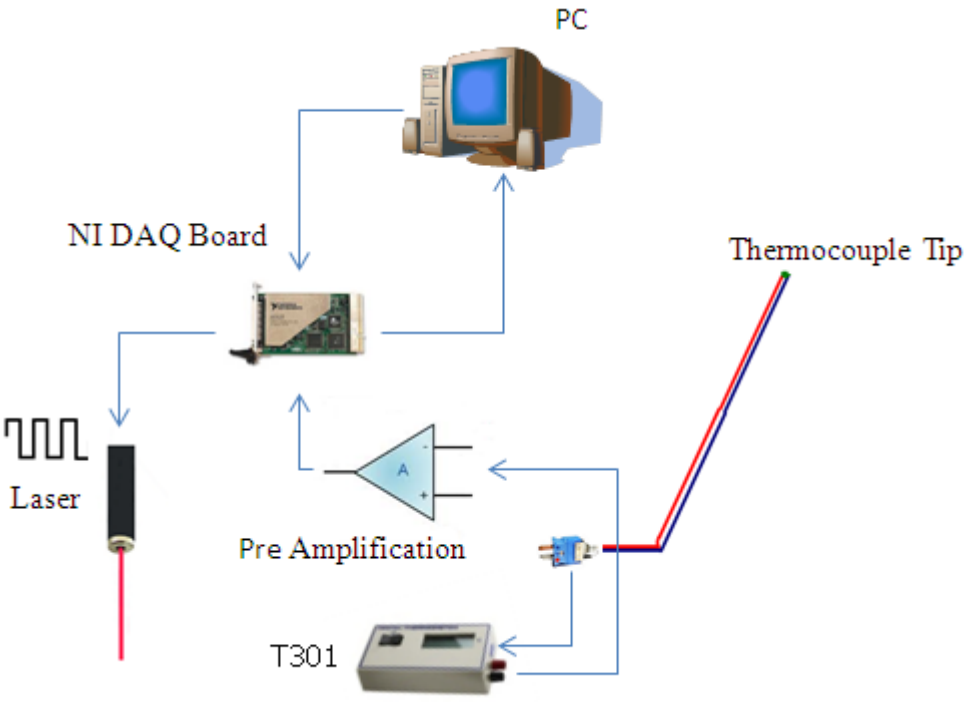

Figure 2.2 Block diagram of the laser control and temperature acquisition into the computer via the NI DAQ Board

2.4.1 Pre-Amplification

A pre-amplification circuit was used between thermocouple output and NI DAQ board to improve signal to noise ratio. The Op-amp circuit is a non-inverting amplifier that has gain of 41. The circuit amplifies the voltage output from T301 and feeds the amplified voltage to the DAQ board. The schematic of circuit is shown in Figure 2.3.

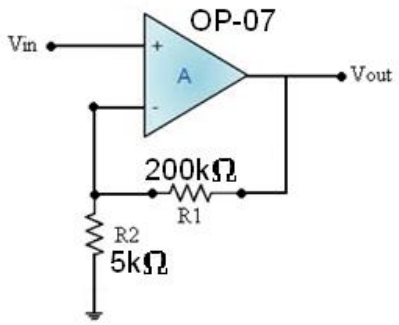

Figure 2.3 A non-inverting amplifier with a gain of 41

2.4.2 DAQ Board

NI PCI 6259 DAQ Board's 1 input and 1 output channels were used in this study. Input was connected to the pre-amplifier`s output and the DAQ output was connected to the laser to control power intensity through the custom Matlab software.

Figure 2.4 NI PCI 6259 DAQ Board, maximum sampling frequency is 1.25 MHz

2.4.3 Custom Software

Data acquisition was controlled by a custom Matlab software designed as a Master thesis at NJIT [37]. In this particular Matlab code (Figure 2.5), user is able to define the train parameters, such as train pulse frequency, pulse width, pulse duration and temperature recording parameters, for instance sampling rate and recording duration. Also, it saves the data as well as the parameter settings to be recalled for data analysis.

Figure 2.5 The Custom Matlab Software User Interface [37]

2.5 Experimental Procedure

The experiments were performed in 350-500g Sprague-Dawley rats. Under deep anesthesia, the head of the animal was immobilized in a stereotaxic frame. The tissue and scalp covering the right hemisphere of cerebrum were removed using surgical instruments. The cranium was opened using rongeurs as a 8x4 mm oval window. The shape and location of skull opening is shown in Figure 2.6.

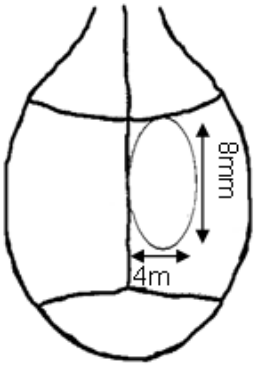

Figure 2.6 Exposed area of the cerebral cortex for temperature measurements in the experimental animals

The thermocouple probe (T301, T type with a tip diameter of 100µm, Unisense, Denmark) was modified to reduce the response time. Probe glass cover was removed and replaced with a thin layer of epoxy (Figure 2.7). The thermocouple wires were run along the shank of a Tungsten electrode as a carrier with a sharp tip for easy penetration into the brain tissue. The probe was attached to a 3-axis manipulator and the penetration was made at an angle of 45 degrees from the horizontal plane. Using the manipulator, temperature probe was inserted into the brain tissue until its tip reached 2mm depth in steps of 250µm in the vertical direction (corresponds to ~350 µm steps in the direction of the probe axis).

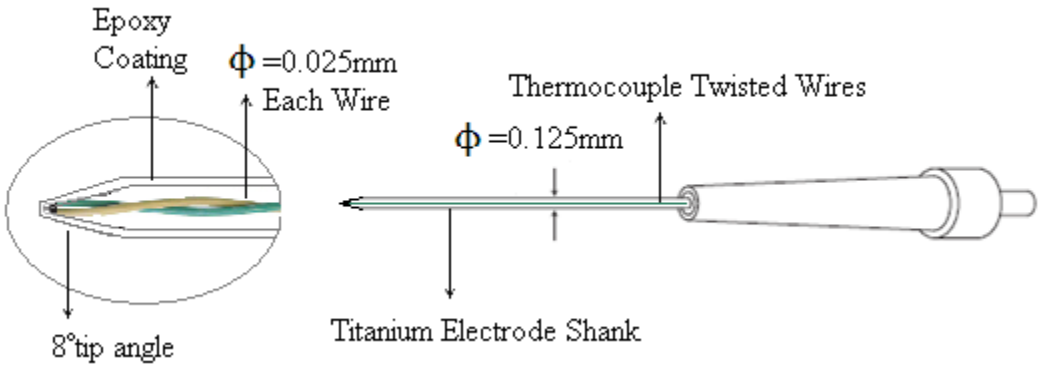

Figure 2.7 The modified thermocouple probe

NIR laser source (DLS-500-830FS-100, StockerYale, Canada, 74 mW) was mounted 13.5 cm above the rat brain surface facing down on the brain (Figure 2.8). Another manipulator was used for laser source displacements in steps of 125 μm in the horizontal direction. The control pulse train (2ms pulse width, 100 Hz, 5s train duration) was sent to laser by custom Matlab program. The footprint of the laser beam was observed on the brain cortex surface as a circle of 0.56 mm in diameter using an NIR paper detector that converts NIR light to visible light. This point where the laser beam hit the thermocouple tip on the brain surface in the middle of oval skull opening was assumed as the origin of 2D coordinates and laser was moved in steps horizontally with respect to this reference point.

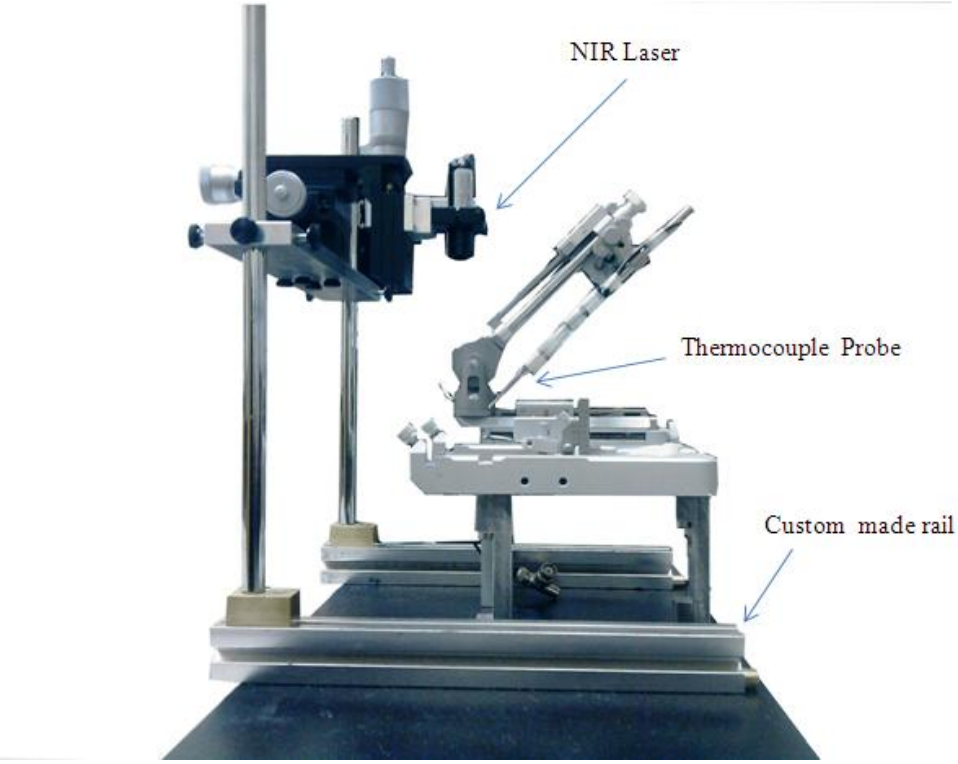

Figure 2.8 Experimental setup including laser, thermocouple and the stereotaxic frame

Vertical displacements of the temperature probe were controlled by moving 3-axis micromanipulator deeper into the tissue as mentioned above, therefore making measurements in a 2D vertical plane sagittally oriented. The total area covered was about 1200 by 2000 µm (horizontal by vertical) with a resolution of 125 µm horizontally and 250 µm vertically.

The laser is controlled by a 100 Hz pulse train which has two frames with duration of 16 seconds each. Each frame has a one second LASER-OFF, a five second LASER-ON, and a ten second LASER-OFF intervals (Figure 2.9). The temperature perturbation due to the laser exposure is shown in the bottom part of Figure 2.9.

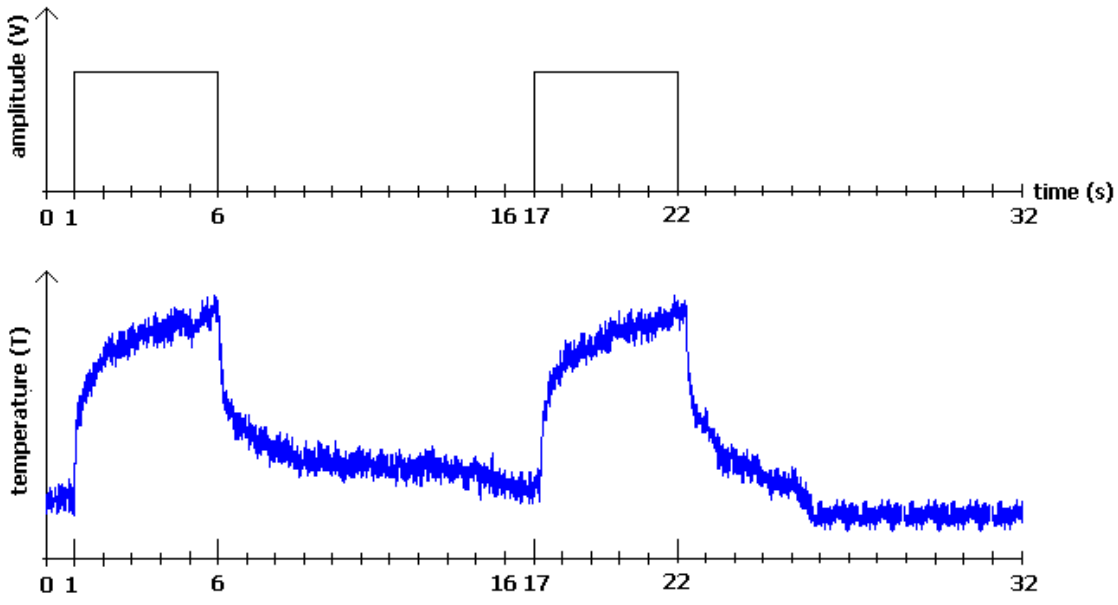

Figure 2.9 The laser control pattern and recorded temperature change

CHAPTER 3

RESULTS and DISCUSSION

3.1 Thermocouple Calibration

The tip of thermocouple is dipped in hot water with a temperature above 50 °C. While the water is cooling down, temperature points and voltage values are recorded. In Figure 3.1 output voltage of the thermocouple is plotted against temperature. A linear line fit to the measurement points had a correlation of R^2=0.999. The input-output relation was found to be y = 5.173 x - 13.71 where x is the temperature in degree Celsius and y is the voltage output in millivolts. The slope of 5.173 mV/°C was slightly larger than the specified value by the manufacturer (5 mV/°C).

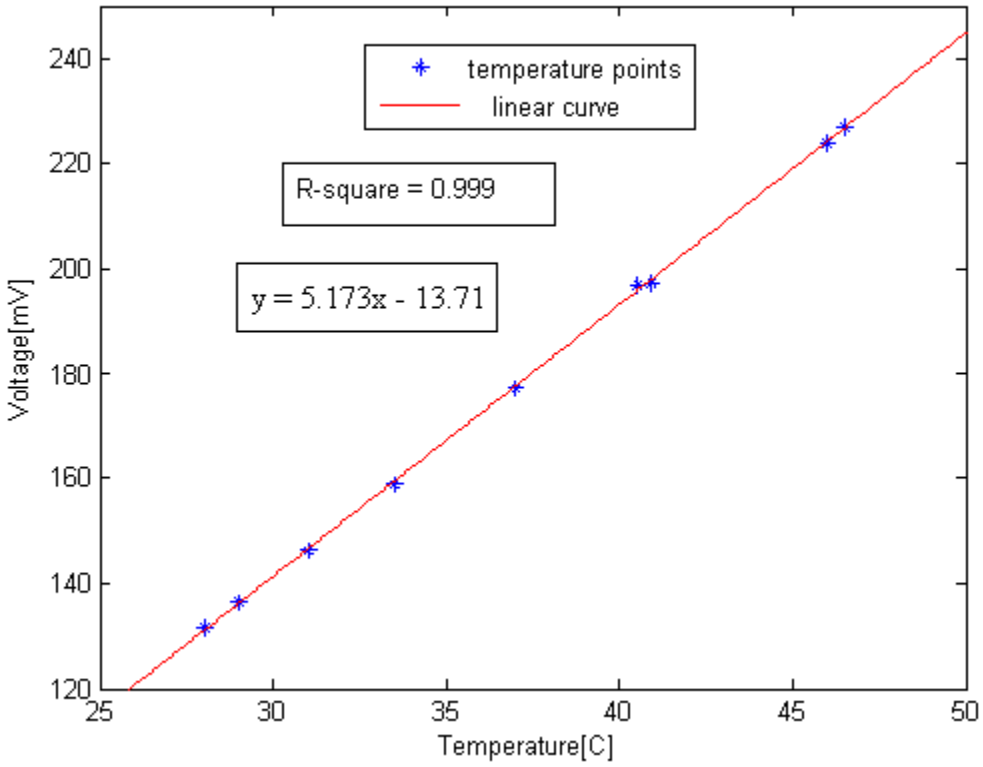

Figure 3.1 Temperature calibration curve

3.2 Laser Calibration

Laser output power directly determines a laser`s ability to perform a process. The NIR laser performance was checked measuring its power with a power meter that was placed at 13.5 cm from the laser. The power meter reading was recorded with respect to control voltage. Figure 3.2 shows that there is a linear correlation of $R^2 = 0.999$ between power meter reading and control voltage of NIR laser. The output power changed from 0 % to 100% as the input voltage decreased from 4.5 V to 0.5 V. The curve had a negative slop, i.e. the output power decreased with input voltage. The input-output relation was described by y = -19.32 x + 86.36 where x is the control voltage in volts and y is the laser power in milliwatts.

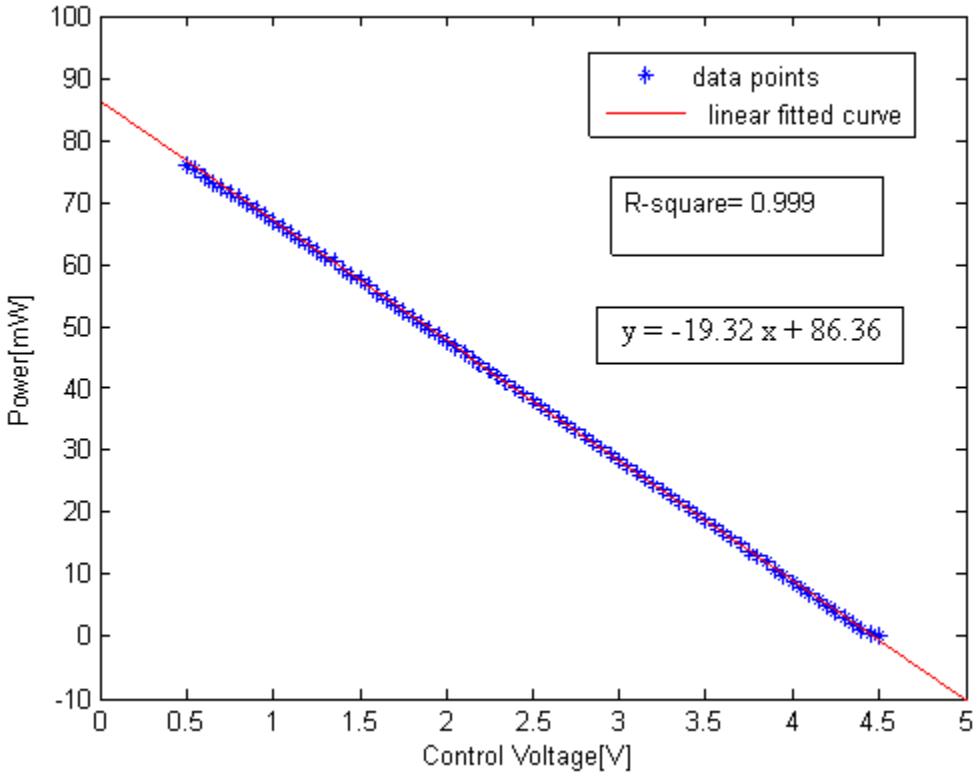

Figure 3.2 Control voltage vs. output power of the laser measured experimentally

3.3 Experimental Results and Discussion

An example of the raw temperature signal is shown in Figure 3.3. This data was collected at a depth of 500 μm from the pia matter surface. The pulse signal has two trains that start at t=1 and t=17 seconds. There is a delay between two trains. The temperature first increases very rapidly from 32 °C and slowly reaches to about 33 °C before the laser power is turned off at t=6 and t=22 seconds.

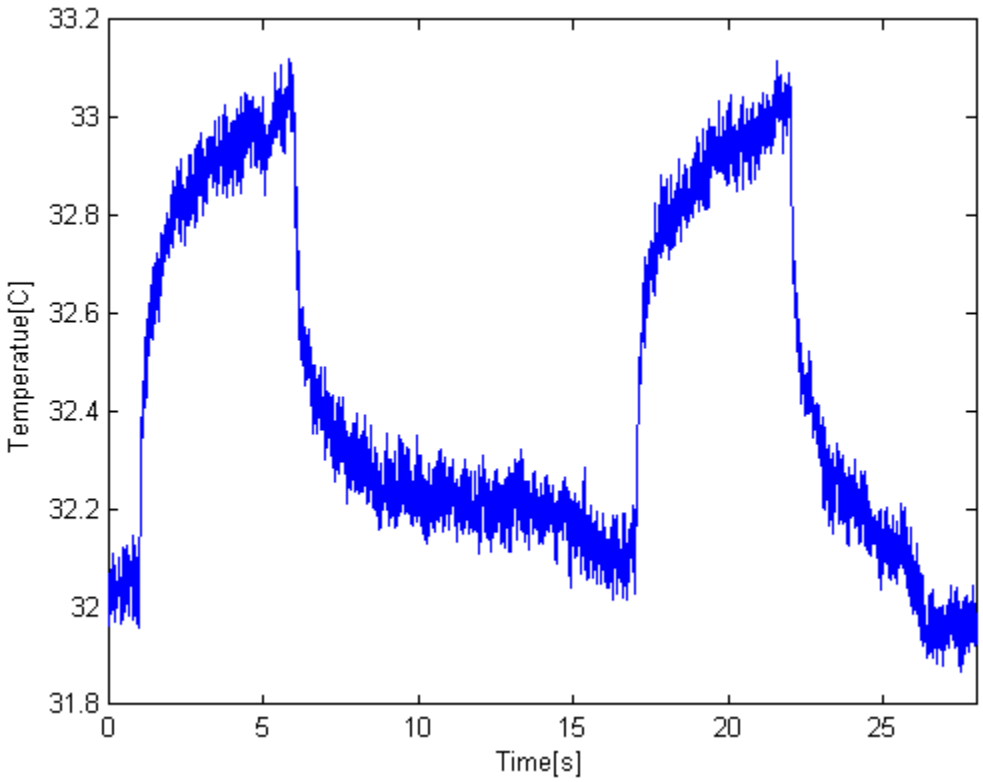

Figure 3.3 An example of raw temperature data collected at a depth of 500 μm

The temperature data were filtered to eliminate noise and high frequency components. After filtering, the temperature data points were marked (Figure 3.4) to obtain temperature elevations due to laser illumination. The data points marked as I and III in Figure 3.4 were calculated by averaging the data points before the laser was turned on (I and III). These values were estimated as our baseline temperature values before

application of the laser pulse. On the other hand, the data points were obtained via linear curve fitting method to the raw data are circled as II and IV in Figure 3.4, respectively. These values were taken as maximum temperature increases from the baseline at the end of the laser pulse (t=6 and t=22 seconds).

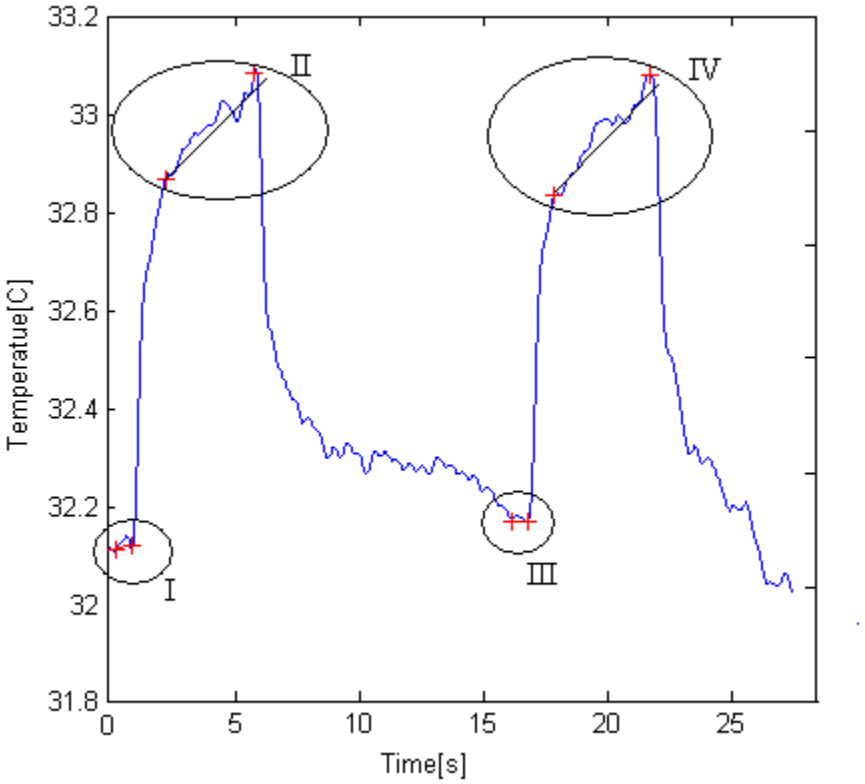

Figure 3.4 The temperature measurements at the beginning and end of the laser pulse

For instance, the minimum and maximum temperature points were measured as 32.1 °C and 33 °C, respectively, for the trial shown in Figure 3.4. Taking these particular temperature points, the temperature difference was obtained 0.9 °C at a depth of 500 µm. As explained in methodology, every single trial was recorded and processed individually.

The study investigated the temperature elevation profile by NIR laser in the sagittal plane. The maps of temperature increase were extracted within 2D vertical plane for the last four experiments individually (Figures 3.5, 3.6, 3.7, and 3.8).

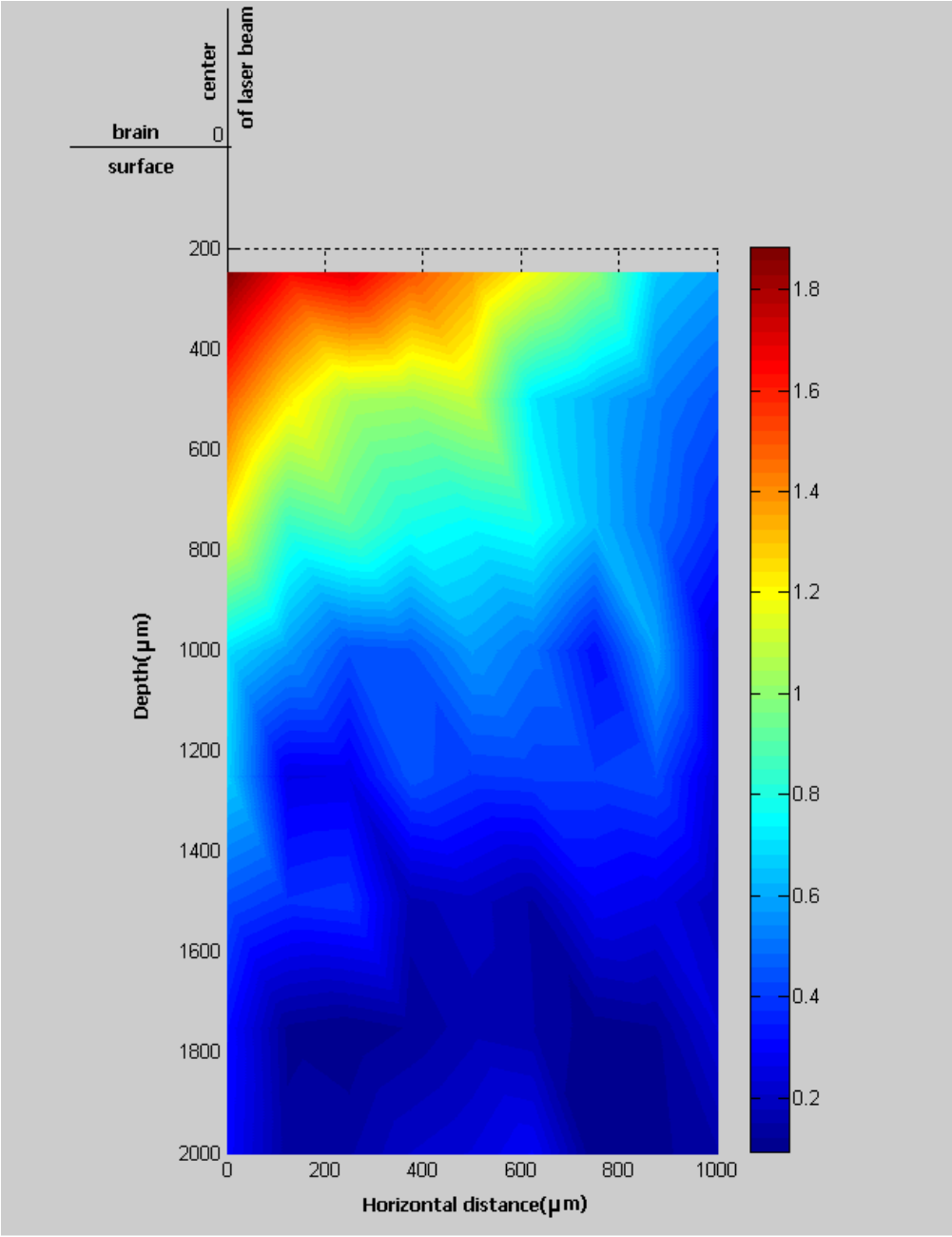

Figure 3.5 The map of temperature elevation in Experiment 5

Only one half of the vertical plane is scanned. The spatial resolution is 125 µm in the horizontal direction and 250 µm in the vertical direction.

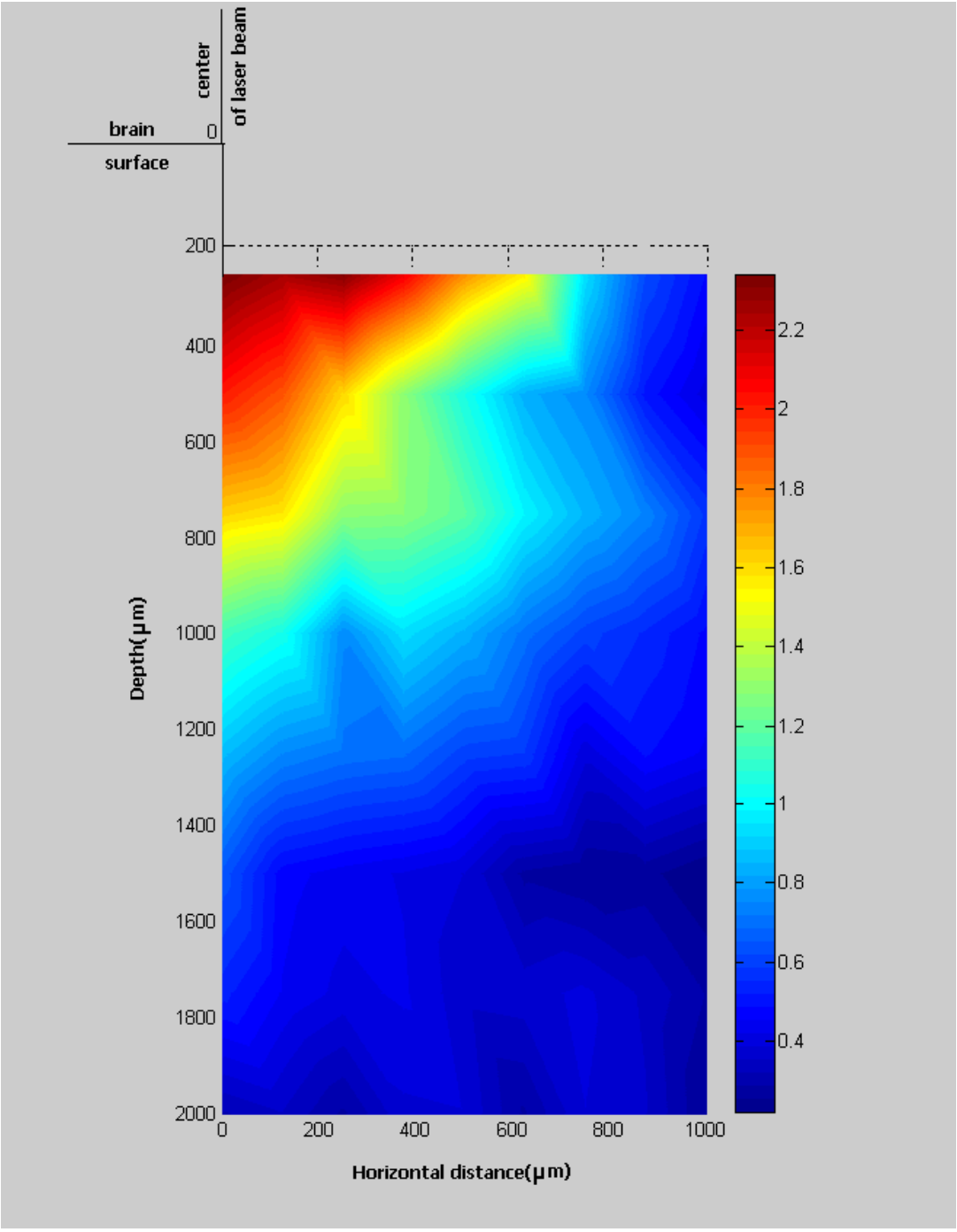

Figure 3.6 The map of temperature elevation in Experiment 6

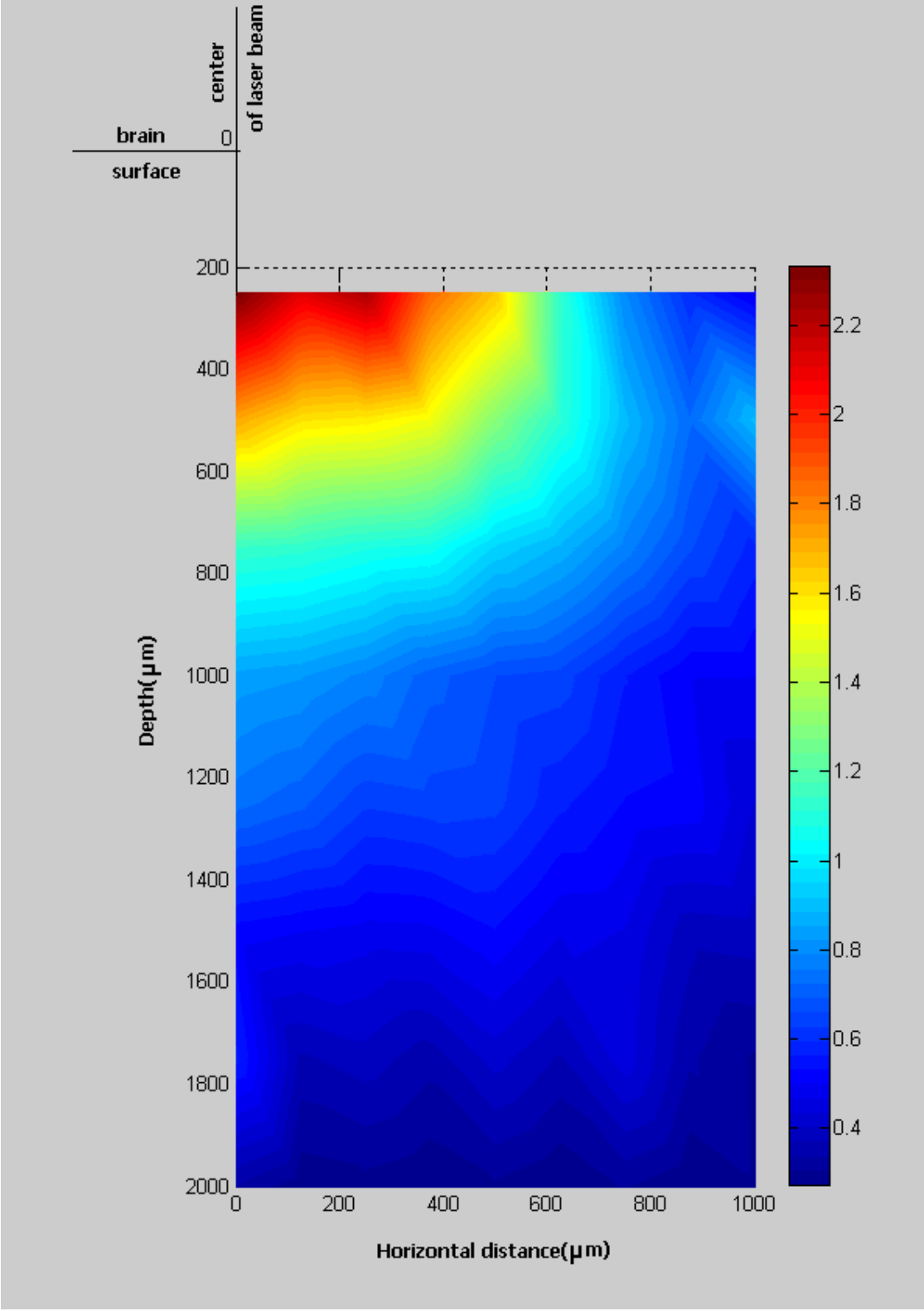

Figure 3.7 The map of temperature elevation in Experiment 7

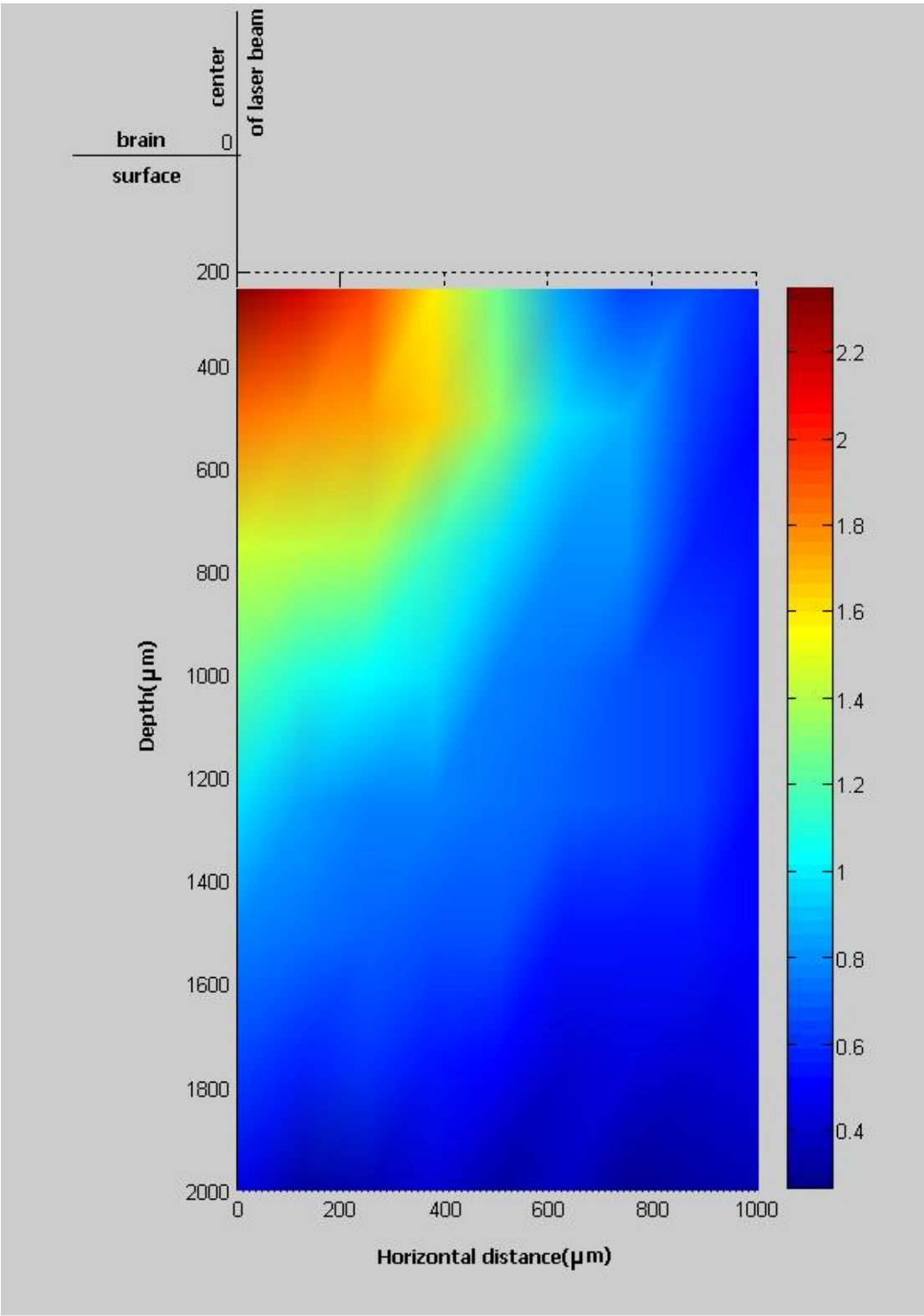

Figure 3.8 The map of temperature elevation in Experiment 8

The temperature points for the same depth and horizontal distance were averaged from last four experiments. The averaged map of temperature is shown in Figure 3.9.

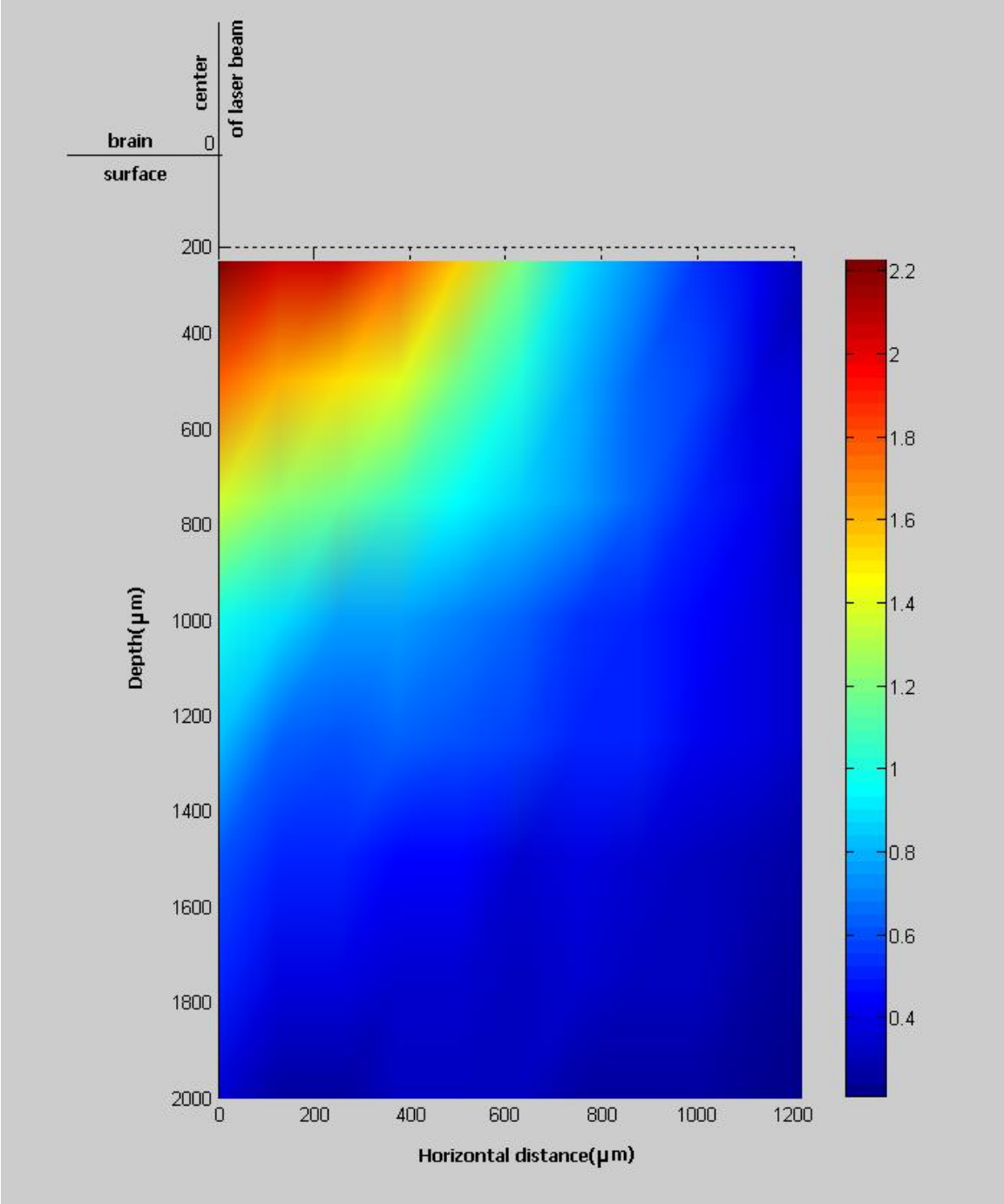

Figure 3.9 The average temperature increase profile of neural tissue in the vertical plane (sagittal) due to laser illumination

Optical properties of neural tissue play an important role in this study. NIR Laser light can penetrate with more ease into neural tissue than visible light. The dominant form of interaction with the neural tissue at NIR wavelength is scattering. Since grey matter has lower scattering coefficient than white matter, NIR light penetrates more readily into the grey matter. Figure 3.9 indicates that the maximum increase of temperature is 2.1 °C at the origin of 2D plane due to laser irradiation at a power of 23 mW. The temperature elevation in a depth of 1000 μm is around 0.9 °C. The same temperature point (0.9 °C) in a horizontal direction occurs at 700 μm. Thus the spatial gradient of temperature decrease is steeper in the horizontal direction in comparison to the decline in the vertical direction. In other words, NIR laser penetration is much stronger in the vertical direction than horizontal direction.

The attenuation of light intensity by depth inside neural tissue was investigated in next. The temperature elevation was measured in steps of 250 μm to the depth of 2000 μm. Figure 3.10 suggests that the temperature elevation was 2.4 °C at a depth of 250 μm and 0.4 °C at a depth of 2000 μm. Measured temperature points were fitted by an exponential curve with a correlation of R^2 = 0.998. In other words, inside the rat brain cortex, the light intensity of NIR laser attenuates exponentially as a function of depth. The depth-temperature elevation relation was found to be y = 2.921 $e^{-0.0008906x}$ where x is the depths in μm and y is the temperature elevations in °C.

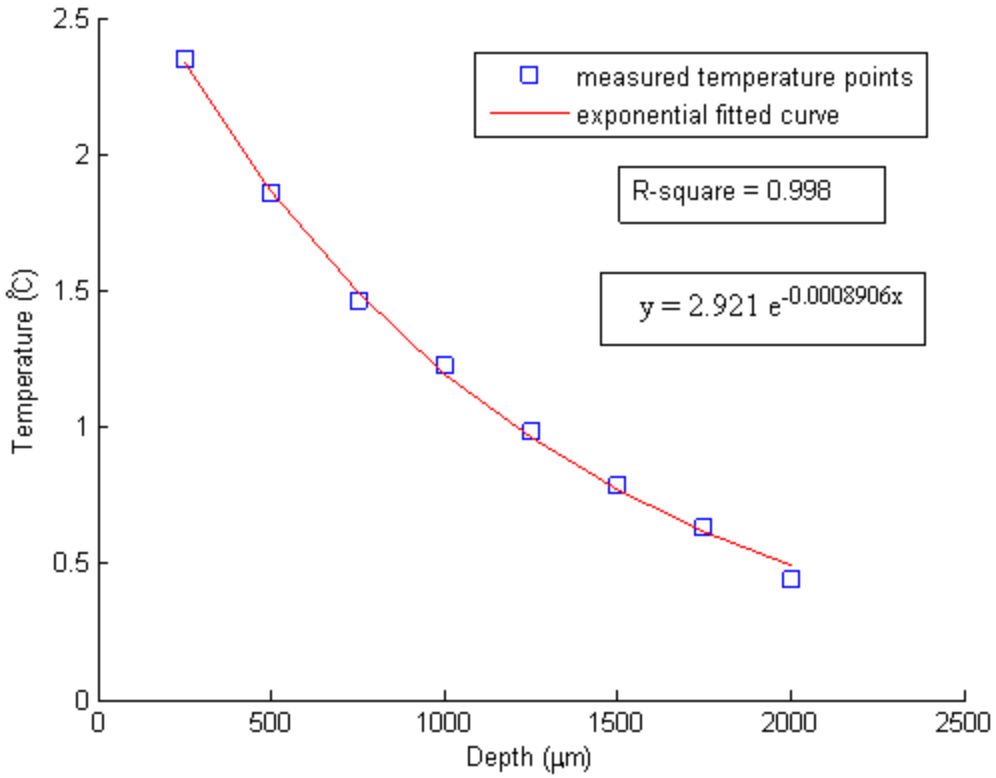

Figure 3.10 The temperature elevation as a function of depth in the rat brain due to NIR laser exposure. The horizontal location corresponds to the center of the laser beam.

3.4 Limitations

In this study, the steady-state was assumed to be reached within five seconds of laser beam exposure. From the time course of the temperature signal however, it was evident that the temperature signal was still slowly changing at the end of the five second pulse train. Moreover, motion artifacts due to breathing and beating of the heart may have contaminated the signal. We have also seen the effects of air circulation in the room in the temperature measurements made near the brain surface. Despite these disturbances, a certain level of reproducibility was achieved in the measurements.

A temperature elevation of 1 °C causes fatal damage in neural tissue and affects the homeostasis [39]. Thus, we would normally consider a conservative value of 0.5 °C as a limiting factor in this project [38]. However, the signal-to-noise ratio from the thermocouple was very poor for small temperature changes. Therefore, we used a much higher laser power level than we intend to use in order to improve the signal-to-noise ratio. We will scale the temperature measurements down, since the temperature-laser power relation is quite linear at low power, in order to find out the laser power limit to keep the temperature elevations below 0.5 °C.

Finally, the heat dissipation through the skull opening into air and through the electrode shank that carries the thermocouple were assumed to be negligible in this study. These assumptions may need to be validated by estimating the heat transfer due to conduction in both cases.

CHAPTER 4

SUMMARY & FUTURE WORK

Infrared irradiation has been used in therapeutic and diagnostic applications such as brain tumor treatments [33], spectroscopic imaging [36], and subretinal prostheses [35]. In these studies the temperature elevation is a complication factor that has to be dealt with. The safe level of NIR exposure is given only for the skin and retina by recently updated American National Standards for Safe of Lasers (ANSI Z136.-2007).

This study is based on temperature elevation in a brain tissue due to NIR laser irradiation. First, we applied the pulse trains at different laser positions along x-axis horizontally and made temperature measurements at different depths to obtain the 2D temperature distributions in the sagittal plane.

Figure 3.9 shows that the highest temperature elevation was 2.1 °C close to the surface at a depth of 250μm where the amount of photons penetrating and getting absorbed in the tissue is presumably at a maximum. The spatial gradient of temperature is smaller vertically than horizontally. This must be due to the directionality of the beam entering the medium in the vertical angle and also, the anisotropy property of neural tissue.

The living tissue tends to protect and maintain the temperature below a certain value despite the heat applied by the NIR laser irradiation. If the temperature exceeds 41-44 °C, it can cause permanent damage in neural tissue. Figure 3.9 indicates that the power of 23 mW causes temperature increase of 2.1 °C at a depth of 250 μm Sailer [35] et. al. reported a temperature rise of 3.2 °C when illuminating a subretinal implant with infrared

power of 15 mW (4.8 mW/mm^2) inside a rabbit's eye. The discrepancy may be explained by the differences in vascularization of the brain and the subretinal tissue.

The laser beam size is an important concern inside neural tissue. Even through the laser source was fixed to a micro-manipulator, the brain moves due to the breathing and the heart beating. The sensitivity to motion can be eliminated both increasing the beam size and thus radiating a larger tissue volume. The beam profile would be considered as a critical factor to keep the temperature below a certain limit which does not cause a permanent damage to the neural tissue. A Gaussian profile of a circular beam has a peak of $1/2\pi\sigma^2$ times the total power of the source. Smaller diameter beam profile can be peaky enough to induce large temperature changes in the center of the beam. A flat profile circular beam that can be obtained with the use of optical microlenses can eliminate the spatial peak effect.

A bioheat model can provide insights as to how NIR laser exposure affects the temperature profile in neural tissue. In addition, a computer model can include a transient time analysis module that would allow one to study the temperature changes as a function of time. Therefore, one can increase the level of confidence in these experimental results by verifying them with a bioheat computer model and studying the effects of various tissue parameters that one cannot have access to in an experimental setup.

Furthermore, the relation between the laser power and the temperature elevation can be investigated using the experimental setup developed in this study. One would normally expect a linear increase in temperature up to a certain power level of the laser. However, some biological phenomena should start taking place at higher temperatures in order to limit the temperature in the tissue and prevent the death of neural cells.

Finally, this experimental paradigm can be applied to other parts of the central nervous system, the white matter in the brain and the spinal cord for instance, to obtain more complete results and interpret them comparatively.

APPENDIX

MATLAB SOURCE CODES FOR THE TEMPERATURE DIFFERENCE DETERMINATION

The matlab source codes for the temperature difference determination are provided below.

```
 answer =1;
    d=1;                    %//trial number  starts
      j=100;                %trial number iteration, in other words trial number
for i=1:j
   j=j+1;
   StrI=int2str(d);
   MatName='trial';
   Mat='.mat';
   temp=strcat(MatName, StrI);
   filename=strcat(temp,Mat);
    load(filename);
T = 100;
% design a filter with fc corner frequency
fc=2;                          % corner frequency of the filter (in Hz)
fs=1000;                       % sampling freq
fn=2*fc/(fs);          % normalize the corner frequence with fs
[b,a]=butter(3,fn);            % design a 3rd order  butterworth filter, low pass
```

```
[h,w] = freqz(b,a,10000);          % this calculates the transfer function at 10000 different points of digital frequency; h is the transfer function at w frequencies
f=w/(2*pi*T);          % convert the digital frequency array to analog frequency in Hz
 filtered_signal=filtfilt(b,a,data(:,1));    %filter signal
 t=1/fs:1/fs:length(data(:,1))/fs; % time axis for plotting
figure;
plot(t,filtered_signal);
hold on;
%picking the points from temperature data
 [x,y] = ginput(8);
 x1=x(1,1);
y1=y(1,1);
plot(x1,y1,'r+');
 x2=x(2,1);
y2=y(2,1);
plot(x2,y2,'r+');
x3=x(3,1);
y3=y(3,1);
plot(x3,y3,'r+');
 x4=x(4,1);
y4=y(4,1);
plot(x4,y4,'r+');
 x5=x(5,1);
```

```
y5=y(5,1);
plot(x5,y5,'r+');
x6=x(6,1);
y6=y(6,1);
plot(x6,y6,'r+');
 x7=x(7,1);
y7=y(7,1);
plot(x7,y7,'r+');
 x8=x(8,1);
y8=y(8,1);
plot(x8,y8,'r+');
 x = x*1000;
 figure;
plot(data);
hold on;
 x1=x(1,1);
y1=y(1,1);
plot(x1,y1,'r+');
 x2=x(2,1);
y2=y(2,1);
plot(x2,y2,'r+');
 x3=x(3,1);
y3=y(3,1);
```

```
plot(x3,y3,'r+');
x4=x(4,1);
y4=y(4,1);
plot(x4,y4,'r+');
 x5=x(5,1);
y5=y(5,1);
plot(x5,y5,'r+');
 x6=x(6,1);
y6=y(6,1);
plot(x6,y6,'r+');
 x7=x(7,1);
y7=y(7,1);
plot(x7,y7,'r+');
x8=x(8,1);
y8=y(8,1);
plot(x8,y8,'r+');
 a_min_1 = mean (data (x1:x2));
 a_min_2 = mean (data (x5:x6));
 y_x= data(x3:x4);
x_y = x3:x4;
x_y = (x_y)';
a_max_1_curve_coef = polyfit(x_y,y_x,1);   % fitting in a curve
a_max_1= a_max_1_curve_coef(1,1) * 6000 + a_max_1_curve_coef(1,2);
```

```
plot(6000,a_max_1,'ro');
hold on
new_curve_1 = a_max_1_curve_coef(1,1)* x_y + a_max_1_curve_coef(1,2);
plot(x_y, new_curve_1,'g');
y_x= data(x7:x8);
x_y = x7:x8;
x_y = (x_y)';
a_max_2_curve_coef = polyfit(x_y,y_x,1);
a_max_2= a_max_2_curve_coef(1,1) * 22000 + a_max_2_curve_coef(1,2);
plot(22000,a_max_2,'ro');
hold on
new_curve_2 = a_max_2_curve_coef(1,1)* x_y + a_max_2_curve_coef(1,2);
plot(x_y, new_curve_2,'g');
  a_dif_1= ((((a_max_1-a_min_1)/41)/5)*1000);
a_dif_2= ((((a_max_2-a_min_2)/41)/5)*1000);
  answer = str2double(input('would you like to save this? (yes/no) (1/0)','s'));
 if answer==1
a_table (d,1) = d;
a_table(d,2) = a_dif_1;
a_table(d,3) = a_dif_2;
  dosya = load ('saved_data_table.txt', 'dosya');
  dosya(d,1) = d;
 dosya(d,2) = a_dif_1;
```

```
 dosya(d,3) = a_dif_2;
  save('saved_data_table.txt', 'dosya', '-ASCII');
       d=d+1;
      else
    if answer==0
%    d = d-1;
    else
        if answer==3
            dosya = load ('saved_data_table.txt', 'dosya');
            save('saved_data_table.txt', 'dosya', '-ASCII');
   break;
        end
    end
end
 end
```

REFERENCES

[1] Neuman, M. (2000). *The Biomedical Engineering Handbook*, *Physical Measurements* (2nd ed.). CRC Press LLC. Boca Raton, FL. (ch. 47).

[2] Thermoelectric Effect. Retrieved November 18, 2011, from http://www.enercorp.com/products/pdf/02w.pdf.

[3] The variation of resistance with temperature. Retrieved November 19, 2011, from http://www.enercorp.com/products/pdf/02w.pdf.

[4] Resistance temperature detectors (RTDs). Retrieved November 19, 2011, from http://sensorwiki.org/doku.php/sensors/temperature.

[5] Thermistors. Retrieved November 19, 2011, from http://www.enercorp.com/products/pdf/02w.pdf.

[6] Kreider K. (1985). *Fiber Optic Thermometry, in Applications of Radiation Thermometry*, *ASTM STP 895*, Philadelphia, PA. American Society of Testing and Materials, J. C. Richmond and David P. DeWitt, (pp. 151–161).

[7] Temperature sensor comparison table. Retrieved November 19, 2011, from http://www.peaksensors.co.uk/comparingthermocouplesrtdsthermistorsandinfrared.htm.

[8] Introduction to Semiconductor Temperature Sensors. Retrieved November 15, 2011, from http://www.capgo.com/Resources/Temperature/Semiconductor/Semi.html.

[9] The AD590, 2-terminal integrated circuit temperature transducer. Retrieved November 15, 2011, from http://www.analog.com/static/imported-files/data_sheets/AD590.pdf.

[10] Principles of Non-Contact Temperature Measurement. Retrieved November 15, 2011, from http://support.fluke.com/rayteksales/Download/Asset/IR_THEORY_55514_ENG_REVB_LR.PDF.

[11] Infrared Thermometer Basics. Retrieved November 15, 2011, from http://www.ehow.com/how-does_4965130_infrared-thermometers-work.html.

[12] Infrared Gun Thermometers. Retrieved November 15, 2011, from http://www.professionalequipment.com/infrared-thermometer/.

[13] Fristrom R. M. (1995). *Flame Structure and Processes*, Oxford University Press, London, UK. (pp.132).

[14] Coherent anti-Stokes Raman spectroscopy, Retrieved November 15, 2011, from http://en.wikipedia.org/wiki/Coherent_anti-Stokes_Raman_spectroscopy.

[15] Rossow, R. (2005). *Blackbody temperature calculations from visible and near-IR spectra for gas-fired furnaces*, University of Missouri, Columbia, MO.

[16] Zundong Y, Tiejun W, Yunig D., Jiyu W., and Qi, Z. (2003) *Precision Photoelectric Pyrometer and Its Calibration, in Temperature: Its Measurement and Control in Science and Industry.* Vol. 7, (pp.559–563). New York, NY.

[17] Derflinger,T. (2011) *Thermal imaging for medical applications*, The Thermogram Center and Dr. Robert Kane, International Academy of Clinical Thermology. Retrieved November 15, 2011, from http://www.medicalir.com.

[18] Near infrared imaging. Retrieved November 15, 2011, from http://www.scholarpedia.org/article/Near_infrared_imaging.

[19] Gaussian mode. Retrieved November 15, 2011, from http://uotechnology.edu.iq/dep-laserandoptoelec-eng/laboratory/Laser%20principles%20lab/(6)Gaussian%20mode.pdf.

[20] Abdo, A., Sahin, M., Freedman, D., Cevik, E., Spuhler, P., Unlu, S. (2011). *Floating light-activated microelectrical stimulators tested in the rat spinal cord*. Journal of Neural Engineering Vol. 8, Num. 5, (pp.1–9).

[21] Bioheat transfer, Retrieved November 15, 2011, from http://www.ece.utexas.edu/~valvano/research/jwv.pdf.

[22] Pennes, H. (1948). Analysis of tissue and arterial blood temperature in the resting human forearm, Journal of applied physiology, Vol. 1, No. 2. (pp. 93–122).

[23] Wissler, J.W. (1998). Pennes 1948 paper revisited, Journal of applied physiology, Vol. 108, (pp. 239–245).

[24] Eberhart R.C., (1999). *Bioheat transfer in blood-perfused tissues and clinical applications of hypothermia*, Annual review of heat transfer. Vol. 9. (pp.1–78).

[25] Siegman, A.E. (1986). *Lasers*. University Science Books, Mill Valley, CA.

[26] Comsol heat transfer module model library, Retrieved November 15, 2011, from http://www.technion.ac.il/docs/comsol/ht/htmodlib.pdf.

[27] Koechner, W. (2006). *Solid- state Laser Engineering*, Springer Science & Business Media, Inc. New York. NY.

[28] Gebhart, S., Lin, W., Mahadevan-Jansen A.(2006). *In vitro determination of normal and neoplastic human brain tissue optical properties using inverse adding doubling*. Phys. Med. Biol Vol. 51. (pp.2011–2027).

[29] Johns, M., Giller, C., German, D., Liu, H. (1996). *Determination of reduced scattering coefficient of biological tissue from a needle-like probe*. Opt. Expr. Vol. 13 (pp.4828–4842).

[30] Ibrahim, T., Abraham, D, Rennaker, R. (2007). *Electromagnetic power absorption and temperature changes due to brain macine interface operation*, Ann. Biomed Eng. Vol. 35. (pp.825–834).

[31] Sharma, H., Hoopes P. (2003). *Hyperthermia induced pathophysiology of the central nervous system*. Int. J Hyperthermia. Vol. 19. (pp.325–354).

[32] Gosalia, K., Weiland, J., Humayun, M., Lazzi, G. (2004). *Thermal elevation in human eye and head die to the operation of a retinal prosthesis*. IEEE Trans. Biomed. Eng. Vol.51. (pp.1469–1477).

[33] Amin, Z., Donald, J., Masters, R., Kant, A. Steger, C., Bown, G., Lees, R. (1993). *Hepatic Metastases: Interstitial Laser Photocoagulation with Real-time US Monitoring and Dynamic CT Evaluation of Treatment*. Radiology. Vol.187.

[34] Elwassif,M., Kong, Q., Vazquez,M., Bikson, M.(2006) *Bio-heat transfer model of deep brain stimulation-induced temperature changes.* Journal of Neural Engineering. Vol. 3.

[35] Sailer, H., Shinoda,K., Blatsios, G., Kohler,K., Bondzio, L., Zrenner, E., Gekeler F. (2007). *Investigating of thermal effects of infrared lasers on the rabbit retina: a study in the course of development of an active subretinal prostheses*. Graefe's Arch Clion Exp Opthalmol. Vol. 245.

[36] Koehler, F., Lee, L., Kidder, H., Lewis, E. (2002). *Near infrared spectroscopy: the practical chemical imaging solution*, Spectroscopy Europe. Vol. 14.

[37] R., Sahu. (2011). *Matlab user interface for neural stimulation and recording applications with a laser control*. M.S.Thesis, Department of Biomedical Engineering, NJIT, Newark,NJ.

[38] Abdo, A., Sahin, M. (2011). *Feasibility of Neural Stimulation with Floating-Light-Activated Microelectrical Stimulators*. IEEE Transactions on biomedical circuits and system. Vol.1. (pp. 1–10).

[39] Sharma, H., Hoopes, P. (2003). *Hyperthermia induced pathophysiology of the central nervous system*. Int. J. Hyperthermia. Vol. 19. (pp.325–354).

[40] Guily, R. (2007). *Stimulating electrode heating effect in neural tissue.* University of California, San Diego, CA.

[41] Bioheat transfer, Retrieved November 18, 2011, from http://kurslab.fysik.lth.se/FED4Medopt/bioheatequation.pdf.